



HAL
open science

Remediation of water contamination using a synergetic system of biochar and photocatalyst: Complete mineralization in simulated real condition

Maroua Abbes, Amine Aymen Assadi, Wided Bouguerra, Lotfi Khezami, Abdeltif Amrane, Abdoulaye Kane, Lotfi Mouni, Elimame Elaloui, Mokhtar Hjiri, H. Zeghioud

► To cite this version:

Maroua Abbes, Amine Aymen Assadi, Wided Bouguerra, Lotfi Khezami, Abdeltif Amrane, et al.. Remediation of water contamination using a synergetic system of biochar and photocatalyst: Complete mineralization in simulated real condition. *Euro-Mediterranean Journal for Environmental Integration*, 2024, 9 (3), pp.1427-1440. 10.1007/s41207-024-00514-2 . hal-04615525

HAL Id: hal-04615525

<https://hal.science/hal-04615525v1>

Submitted on 4 Sep 2024

HAL is a multi-disciplinary open access archive for the deposit and dissemination of scientific research documents, whether they are published or not. The documents may come from teaching and research institutions in France or abroad, or from public or private research centers.

L'archive ouverte pluridisciplinaire **HAL**, est destinée au dépôt et à la diffusion de documents scientifiques de niveau recherche, publiés ou non, émanant des établissements d'enseignement et de recherche français ou étrangers, des laboratoires publics ou privés.

Remediation of water contamination using a synergetic system of biochar and photocatalyst: Complete mineralization in simulated real condition

Maroua Abbas^{1,2}, Amine Aymen Assadi^{3,4*}, Wided Bouguerra¹, Lotfi Khezami⁵, Abdeltif Amrane⁴, Abdoulaye Kane², Lotfi Mouni⁶, Elimame Elaloui¹, Mokhtar Hjiri⁷, and Hicham Zeghioud^{2*}

¹Laboratory of Materials Application to Water, Environment and Energy (LAM3E). Faculty of Sciences of Gafsa – University of Gafsa, Sidi Ahmed Zarroug University Campus - 2112 Gafsa, Tunisia

²UniLaSalle-Ecole des Métiers de l'Environnement, Cyclann, Campus de Ker Lann, 35170 Bruz, France

³ College of Engineering, Imam Mohammad Ibn Saud Islamic University, IMSIU, Riyadh 11432, Saudi Arabia

⁴Université de Rennes, Ecole Nationale Supérieure de Chimie de Rennes, CNRS, ISCR - UMR 6226, F-35000 Rennes, France

⁵ Chemistry Department, College of Science, Imam Mohammad Ibn Saud Islamic University (IMSIU), Riyadh 11432, Saudi Arabia

⁶Laboratoire de Gestion et Valorisation des Ressources Naturelles et Assurance Qualité. Faculté SNVST, Université de Bouira, 100000 Bouira, Algeria.

⁷Department of Physics, College of Sciences, Imam Mohammad Ibn Saud Islamic University (IMISU), Riyadh, 11623, Saudi Arabia

*Correspondence: authors. (AAA) Tel: +966(0)563260210, E-mail: AAAssadi@imamu.edu.sa ; (NT.P) E-mail : hicheming@yahoo.fr

Abstract: Water is a vital source of life in the world and must be preserved for the future. However, this source has been threatened by unrestrained pollution owing to industrialization. Therefore, water treatment techniques must be considered. Bifunctional technology, such as combined adsorption and photocatalysis, is considered among these processes. Photocatalysis in the presence of external UV alters properties and neutralizes substances like dyes. However, a complete mineralization still needs to be achieved. Therefore, this process is combined with biochar-mediated adsorption to facilitate electron-hole separation and dye adsorption on the photocatalyst surface based on the synergetic effects with this composite system. In this study, bark biochar and TiO₂ impregnated on cellulose fiber were elaborated. Prepared biochar was characterized by scanning electron microscopy

(SEM) and energy dispersive spectroscopy (EDS). The adsorbing performance of these materials was evaluated by estimating the elimination of Methyl Orange (MO) in pure water with the presence of different metal ions. Remarkably, 100% MO (6 mg/mL) removal was achieved by adsorption as pretreatment followed by photocatalysis at 6 hours of each step at neutral pH with 80 mg/mL of biochar dose. Metal ions' presence played a vital role during the adsorption and decomposition of MO. CuCl_2 notably enhanced the oxidative/adsorption performance, potentially facilitating photogenerated charge separation and promoting interface formation between CuCl_2 and TiO_2 . To achieve complete methyl orange (MO) removal using 100 mg of biochar, a concentration of 2 ppm CuCl_2 was found to be necessary, with a reaction time of 3 hours. Additionally, the decomposition process of methyl orange was examined and fitted to the pseudo-first-order model.

Keywords: Adsorption; photocatalysis; biochar; combined process; water remediation

1. Introduction

Water is essential for life and human activity, constituting a critical component of the mineral and organic worlds. In modern society, water is intertwined with all daily activities, whether domestic, industrial, or agricultural, and it is increasingly vulnerable to various forms of pollution. This pollution threatens the availability of clean drinking water resources [1]. Consequently, there is a growing demand for the reuse and recycling of water for both industrial processes and drinking purposes. Contaminated water often contains diverse pollutants, including organic dyes [2], pharmaceuticals [3], petroleum hydrocarbons [4], and carcinogenic heavy metals [5], all of which have been quantified at varying concentrations. Numerous techniques are employed for water treatment, encompassing electrochemical methods [6], electrocoagulation [7], the photo Fenton process [8], adsorption [9], membrane separation [10], photocatalysis [11, 12], and combined processes [13, 14]. For instance, the textile industry discharges substantial quantities of wastewater into rivers, leading to various problems, such as increased chemical oxygen demand (COD) and toxicity. However, the most concerning consequence is the substantial reduction in light transmittance, which can harm aquatic plants by interfering with their photosynthetic machinery.

Moreover, environmental dyes exhibit mild to severe toxic effects on human health, including carcinogenic, mutagenic, allergic, dermatitis effects, and kidney diseases [15]. Consequently, research efforts in the Dye Removal field are ongoing, with various physicochemical and biological treatment techniques employed to degrade dye molecules. Among these technologies, adsorption and photocatalysis have gained significant attention due to their ability to minimize waste production [16].

Adsorption is recognized as one of the most effective methods for removing contaminants from gas and wastewater streams [14]. During adsorption, ions of the adsorbate adhere to a solid surface known as the adsorbent. These interactions are predominantly electrostatic [1]. The choice of adsorbent hinges on numerous criteria, including its adsorption capacity and kinetics. Adsorbents facilitate component separation by binding them to surfaces. Widely used industrial adsorbents include activated carbon, silica gels, zeolites, and biochar. Biochar, in particular, has garnered substantial interest due to its capacity to effectively remove various pollutants and its attractive attributes, such as high specific surface area, notable cation exchange capacity [17][18][19], and cost-effectiveness [20][21].

Additionally, biochar can be employed for the removal of heavy metals, pesticides, and phenolic compounds from contaminated soil [21][22][23]. It is characterized by its high porosity and carbon-rich composition, produced through biomass carbonization in an oxygen-poor environment [24]. The efficiency of organic compound adsorption onto biochar primarily relies on interactions such as π - π interactions, electrostatic interactions, segregation, hydrophobic interactions, pore filling, and hydrogen bond formation [25]. Due to its specific surface area, functional surface groups, structural stability, and elemental composition, biochar finds extensive applications across various fields [26]. Thorough material characterization is essential before applying biochar to understand the relationship between biochar production conditions and adsorbate removal efficiency [27][28]. Methyl orange (MO), an organic anionic azo dye, is one of the most widely used dyes globally, accounting for approximately 70% of dye consumption. It is commonly employed in textiles, paper, food, and printing [29]. However, its presence in aquatic environments has adverse effects on wildlife and contributes to numerous diseases, underscoring the importance of its treatment [30].

Removing pollutants from wastewater is critical for environmental conservation and water reclamation. Over recent decades, photocatalytic technology has emerged as

an effective solution to address water pollution challenges. It has garnered substantial attention due to its cost-effectiveness and high efficiency [31][32][33]. Photocatalysis employs catalysts and UV/visible light to degrade pollutants [34]. When the catalyst is exposed to light, it triggers the excitation of electrons from the valence band to higher energy levels, generating reactive oxygen species (RSO) [35]. These RSOs then react with dyes, oxidizing and breaking them down. Catalysts used for pollutant decomposition include TiO_2 , Cu_2O , and BiOCl [11][12][36][37]. An adsorbent like biochar can be added for optimal pigment removal results to create an effective photocatalytic system [38]. To maximize removal rates, combining photocatalysis and adsorption, using TiO_2 as the catalyst and biochar as the adsorbent, proves to be more efficient and cost-effective [39]. In this context, an integrated photocatalysis/adsorption strategy presents a promising approach, harnessing the strengths of both methods. Additionally, the synergistic effects of adsorption and photocatalysis enhance the efficient contact between target pollutants and the reactants generated by free radicals [40].

The primary objective of this study is to develop an efficient method for completely removing methyl orange by combining adsorption with photocatalysis, utilizing biochar as the adsorbent. The kinetics of each technique were separately investigated and further supported by theoretical calculations and fitting. Various configurations of the combined process were explored, including i) adsorption followed by photocatalysis, ii) photocatalysis followed by adsorption, and iii) simultaneous adsorption and photocatalysis. Two different treatment durations, 3 and 6 hours, were also examined for each configuration. Furthermore, the impact of water types (pure, deionized, and tap water) on the efficiency of methyl orange removal was investigated.

2. Materials and Methods

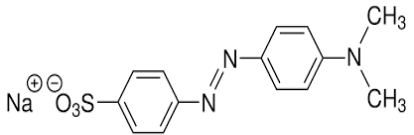
2.1. Reagents

The chemicals used for this study were purchased from high-purity analytical grade: Methyl orange was purchased from Labkem (Barcelona, Spain), chemical formula $\text{C}_{14}\text{H}_{14}\text{N}_3\text{NaO}_3\text{S}$, molar mass ($M= 327.34 \text{ g/mol}$), acid sulfide 96% chemical formula H_2SO_4 , molar mass ($M= 98.08 \text{ g/mol}$) was obtained from PanReac (Darmstadt, Germany), sodium chloride (NaCl)Zinc chloride (ZnCl_2) $\geq 99.9 \%$, $M= 58.44 \text{ g/mol}$ purchased from VWR CHEMICALS Geldenaaksebaan, ($\text{ZnCl}_2 \geq 98 \%$, molar mass

(M= 136.30 g/mol), purchased from SIGMA-ALDRICH), Strontium chloride hexahydrate (SrCl₂.6H₂O), molar mass (M=266.62 g/mol) purchased from SIGMA-ALDRICH, made in Germany, Darmstadt), Magnesium chloride hexahydrate, chemical formula Cl₂Mg .6H₂O ≥ 99.4 %, molar mass (M= 203.30 g/mol) was obtained from VWR CHEMICALS (Geldenaaksebaan, Belgium), copper(II)chloride dihydrate, chemical formula Cl₂Cu.2H₂O, purchased from SIGMA-ALDRICH, Ultra-pure water (Resistivity is 18.2 MΩ.cm, TOC < 10 ppb) used throughout the work. All chemicals used in this work were of commercial analytical quality.

The properties and characteristics of MO are listed in Table 1. Distilled water is used to prepare all the solutions.

Table 1. Physico-chemical properties of Methyl Orange.

Dye name	Chemical formula	Structure	λ max
Methyl Orange	C ₁₄ H ₁₄ N ₃ Na O ₃ S		463.50 nm

λ_{max}: maximum adsorption wavelength of MO

2.2. Bark Biochar and TiO₂ impregnated cellulose fibers preparation

This study used Bark biochar as an adsorbent and was prepared by carbonization according to the protocol of Kaetzi et al [41]. The TiO₂ impregnation on cellulose fiber was described in detail with characterization in our published work by Zeghioud et al [42].

2.3. Photolysis and Photo catalytic Treatment

Methyl orange stock solution was prepared by dissolving 1 g into 1 L ultrapure water under dark conditions. The MO stock solution was used to prepare various concentrations (3, 6, and 8 mg/L) depending on the experimental conditions. Photolysis experiments were performed in a 1 L reactor under UV radiation (12 W) with continuous stirring (1000 rpm). For photocatalytic experiments, a TiO₂-supported photocatalyst sheet was immersed in MO solution and continuously stirred under dark conditions for 60 min to reach adsorption-desorption equilibrium. And then, UV-C irradiation (12 W) was applied. At regular intervals, 3 ml sample solution was

withdrawn using a syringe, filtered through a microporous membrane (0.45 μm), and measured using UV-Vis light spectroscopy (SHIMADZU UV-1800) at a fixed wavelength of 463.5 nm.

The MO degradation rate is calculated using the Eq. 1.

$$\text{Photodegradation efficiency (\%)} = \frac{C_0 - C_t}{C_0} * 100 \quad (1)$$

C_0 and C_t are MO concentrations at time $t=0$ and at any time t of photocatalytic treatment, respectively.

2.4. Adsorption treatment

Two biochar masses (80 and 100 mg) were used for adsorption experiments. Each mass was mixed with 100 mL of 6 ppm MO solution and stirred continuously for 3 hours. Adsorptive removal efficiency MO was determined using Eq. 2. Samples are withdrawn every hour with a syringe, filtered through a microporous membrane (0.45 nm) before analyzing with UV-vis spectra. The removal efficiency was calculated according to the following equation:

$$\text{Adsorption removal efficiency (\%)} = \frac{C_0 - C_t}{C_0} * 100 \quad (2)$$

The MO adsorption capacity of biochar is given by the following equation:

$$q_t = \frac{(C_0 - C_t) V}{m} \quad (3)$$

Where q_t (mg/g) is the quantity of MO adsorbed at time t , V (L) is the volume of the solution, m (g) is the mass of adsorbent, C_0 and C_t are the initial and is the concentration at any time to the MO (mg/L), respectively.

Kinetic studies were conducted by recording the adsorption capacity with contact time from 0 to 200 min, while adsorption isotherms were investigated at initial dye concentrations of 3 to 8(mg/L).

As shown in Table 2, the adsorption kinetic data were described using four kinetics models the first-order kinetic second-order, Elovich, and intra-particle diffusion models [28].

Table 2. Nonlinear kinetic models and their formulas.

Models	Non-Linear formula	Description of parameters
First-order kinetic	$q_t = q_e [1 - \exp(-K_1 t)]$	K_1 (L/min): pseudo-first-order kinetic rate

		constant
Second-order kinetic	$q_t = \frac{q_e^2 K_2 t}{1 + q_e K_2 t}$	K_2 (g/mg.min): pseudo-second-order kinetic rate constant
Elovich	$q_t = \frac{1}{\beta} \ln(1 + \alpha\beta t)$	α : initial adsorption β : Desorption constant
Intra-particle diffusion (IPD)	$q_t = k_{int}\sqrt{t} + c$	K_{int} : rate constant C: intercept

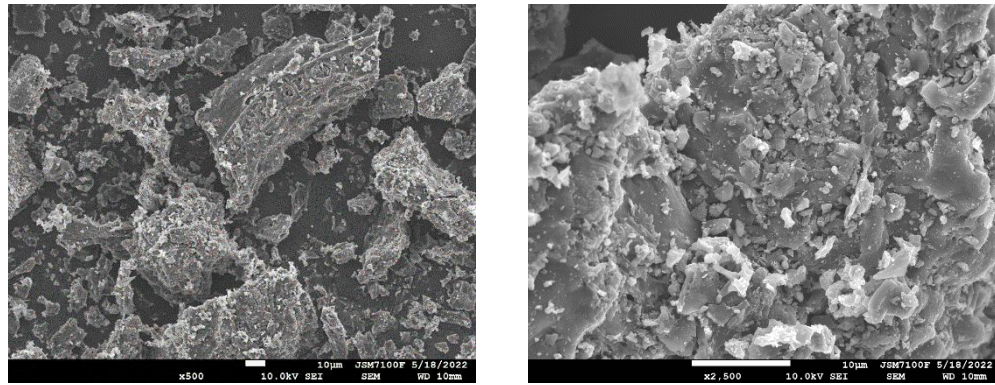
2.5. Combined process: adsorption-photocatalysis

A biochar mixed TiO₂ supported cellulose was used as an adsorbent. About 100 mg of catalyst was added into the 6 mg/L MO solution (total volume 1 L) and experiment was continued for 3 h and the removal efficiency was calculated using Eq. 2.

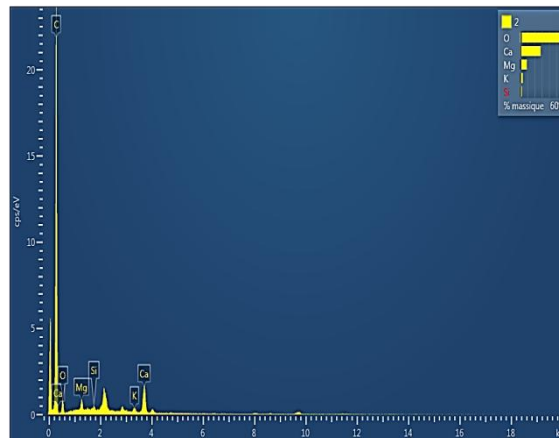
3. Results and discussion

3.1. Material characterization

Several analytic techniques have been deployed to characterize the biochar composition, morphology, and surface properties. The EDS spectrum corresponding to biochar is illustrated in Figure 1b. The spectrum reveals a high carbon content due to biochar's abundance of inorganic elements [43]. This result indicates that biochar may adsorb pollutants more efficiently [43]. Biochar efficiently absorbs impurities from water, but is more effective in carbon sequestration applications [43]. Scanning electron microscopy (SEM) microscopic observations of a sample of biochar tissue (Fig. 1a) gave an idea of their three-dimensional structure. The surface becomes porous, and rigorous structures are typical of biochar. Morphological features reported by other authors show uneven surface ridges characteristic of biochar derived from woody biomass [44, 45]. However, as the content of biochar in the matrix increased, the surface porosity decreased because the biochar filled the pores. A compact and durable material was obtained. Generally, the change in the surface morphology of biochar with a more porous surface provides a larger specific surface area of biochar. The structure is spongy, with many pores. Biochar can offer excellent adsorption capacity [46]. Bark biochar presents 263.45 m²/g of specific surface area with 0.1211 nm of average diameter.



(a)



(b)

Figure 1. (a) SEM image and (b) EDS spectra of biochar.

3.2. Adsorption and photo catalytic kinetics study

Kinetic results of MO adsorption and photocatalytic degradation are shown in Figures 2 and 3, respectively. The graph shows that adsorption capacities increase with time, sharply increasing in the first 60 minutes. This phenomenon is due to the abundant adsorption sites of biochar [47]. The adsorption kinetics of MO on bark biochar was modeled to determine the equilibrium adsorption capacity and the mechanism of this phenomenon.

3.2.1. Adsorption Kinetics study

In this study, four kinetics models were employed to elucidate the kinetics of methyl orange (MO) removal: (i) a pseudo-first-order model (PFO), (ii) a pseudo-second-order model (PSO), (iii) an intra-particle diffusion model (ID), and (iv) an Elovich model [48].

The validity of the kinetic model is confirmed by the values of the correlation coefficient R^2 and by comparing the calculated maximum adsorption capacity (q_m) with the experimental value (q_{exp}) depicted in Table 3.

As indicated in Table 3, the PFO and PSO models exhibit high correlation coefficients, ranging from 0.96 to 0.99 for PFO and 0.97 to 0.99 for PSO. Notably, the maximum adsorption capacity (q_m) calculated using the PFO model closely aligns with the experimental adsorption capacity across all tested concentrations. This finding suggests that MO adsorption predominantly involves physical interactions between MO molecules and the functional groups present on the surface of bark-derived biochar [49]. In contrast, the pseudo-second-order model (PSO) implies that the interaction between MO molecules (adsorbates) and biochar (adsorbent) is more chemisorptive in nature. This phenomenon is evident from the high R^2 values and the calculated q_m values.

For the intraparticle diffusion model, the correlation coefficient (R^2) values range from 0.94 to 0.98, indicating a relatively weak correlation [48], Figure 2b provides further insight. It illustrates that the adsorption of methyl orange by biochar can be divided into two distinct stages. The initial stage, marked by stronger adsorption, is more relevant for MO mass transport over longer distances, as indicated by the larger area under the curve [50]. The second stage involves gradual adsorption and the establishment of equilibrium [51]. The Elovich model, widely used in sorption chemistry for breaking chemical bonds, was also considered in this study [52]. As shown in Table 3, all R^2 values are very close to the unit, suggesting an excellent fit of MO adsorption experimental data to the Elovich model [53].

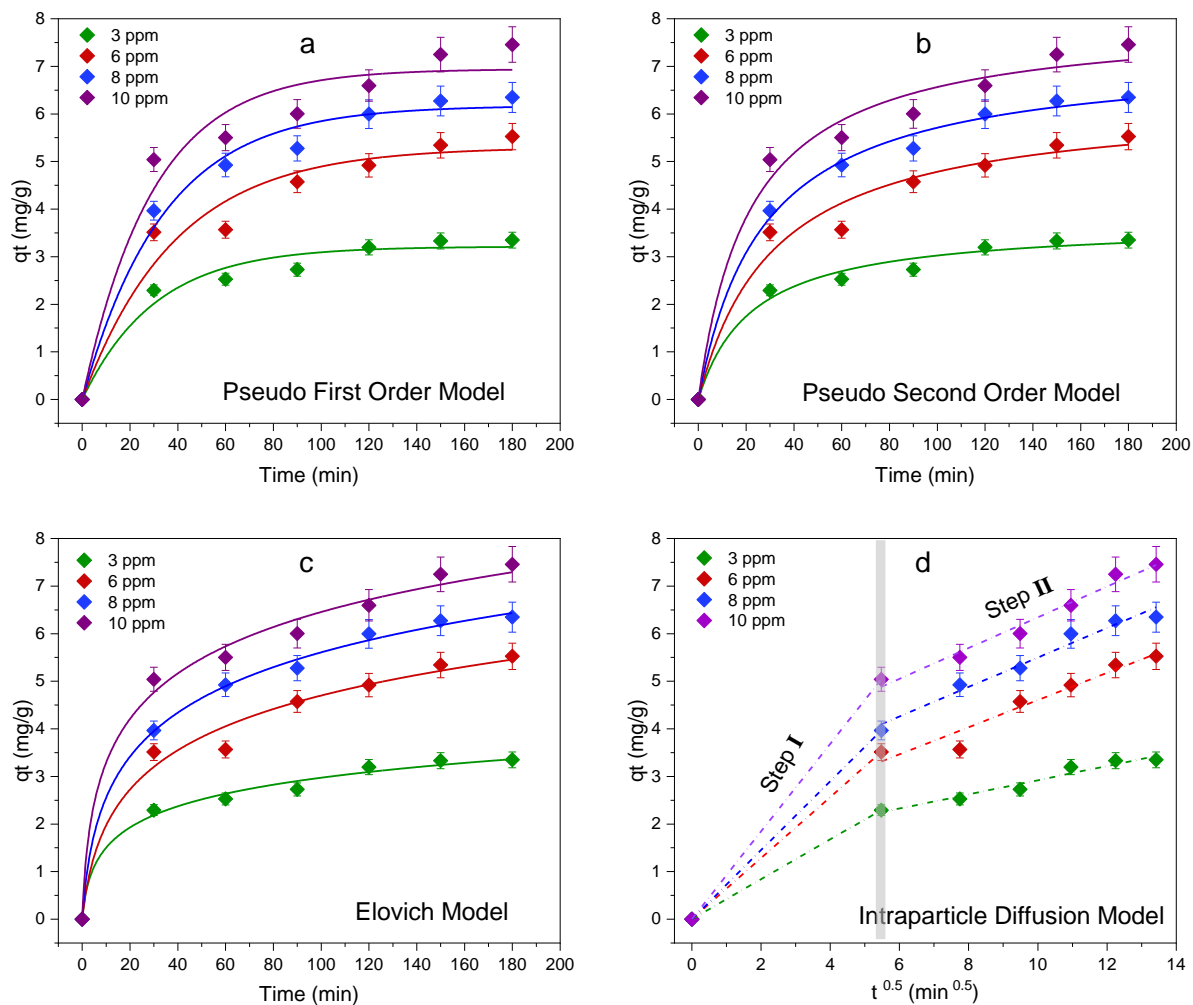


Figure 2. Adsorption kinetics modeling at different initial concentration of methyl orange (biochar dose: 80 mg/100 mL, natural pH).

The constants of each model following the simulation are presented in Table 3.

Table 3. Non-linear Kinetics models and their corresponding parameters.

C_0	q_{exp} (mg/g)	Pseudo first order			Pseudo second order			Intraparticle diffusion				Elovich				
		R^2	q_m	k_1	R^2	q_m	k_2	R^2	K_1	C_1	R^2	K_2	C_2	R^2	B	α
3 ppm	3.35	0.97	3.21	0.033	0.98	3.70	0.012	1.00	0.12	0	0.95	0.15	1.43	0.99	1.5	0.57
6 ppm	5.52	0.96	5.3	0.026	0.97	6.29	0.005	1.00	0.64	0	0.94	0.29	1.75	0.98	0.76	0.46
8 ppm	6.35	0.99	6.17	0.029	0.99	7.25	0.005	1.00	0.72	0	0.97	0.31	2.4	0.99	0.70	0.71
10 ppm	7.46	0.96	6.940	0.034	0.98	8.00	0.006	1.00	0.92	0	0.98	0.23	3.11	0.99	0.70	1.28

3.2.2. Photocatalytic kinetics study

Before initiating the photocatalytic experiment, the catalyst loaded in the aqueous MO solution was subjected to continuous stirring in the dark for 1 hour to achieve adsorption-desorption equilibrium. It is well known that in photocatalysis two distinct and successive stages can occur; adsorption onto the metal oxide surface (active site), and decomposition. The adsorption process can occur directly or through electrostatic interactions [54]. Previous research has reported a direct binding between MO and TiO_2 [55], where MO is an electrically attractive group that may potentially inhibit photocatalysis [56]. It's worth mentioning that MO, being an anionic dye, exhibits strong adsorption characteristics in acidic media [57]. In fact, the color changes as you raise or lower the pH. At acidic pH, methyl orange turns red. At basic pH, methyl orange turns yellow.

Three different MO concentrations (ranging from 3 to 8 ppm) were examined utilizing a cellulose-supported catalyst. Figure 3 illustrates that the decomposition rate of MO decreases as its concentration in the solution increases. This phenomenon aligns with findings from previous research by Nguyen et al. [58]. Within 150 minutes under UV light, the decomposition efficiency of MO notably improved, rising from 9.2% for an 8-ppm concentration to 41.5% for a 3-ppm concentration. This improvement is attributed to the accelerated reaction rate at lower dye concentrations. At higher concentrations, the solute's quantity becomes substantial about the total solvent volume, leading to random particle movement within the solution. This result hinders effective mass transfer. Additionally, high dye concentrations result in increased medium opacity, restricting UV light penetration onto the catalyst surface. Conversely, at lower concentrations, some collisions are more effective, enabling better illumination of the catalyst surface and, thus, a substantial increase in the production of reactive oxygen species (ROS) [59]. The inverse relationship between MO concentration and its removal rate may be attributed to the reduced light penetration due to increased medium opacity. Furthermore, higher dye concentrations tend to promote light absorption by the dye molecules, diminishing the amount of light reaching the catalyst surface and consequently reducing the generation of active sites [49, 60]. At elevated dye concentrations, the desorption rate may also slow down due to the oxidation potential of h^+ ions or the creation of valence band holes, leading to the degradation of organic molecules. Moreover, variations in the number of available active sites could play a role when employing the same catalyst for different dye concentrations [60].

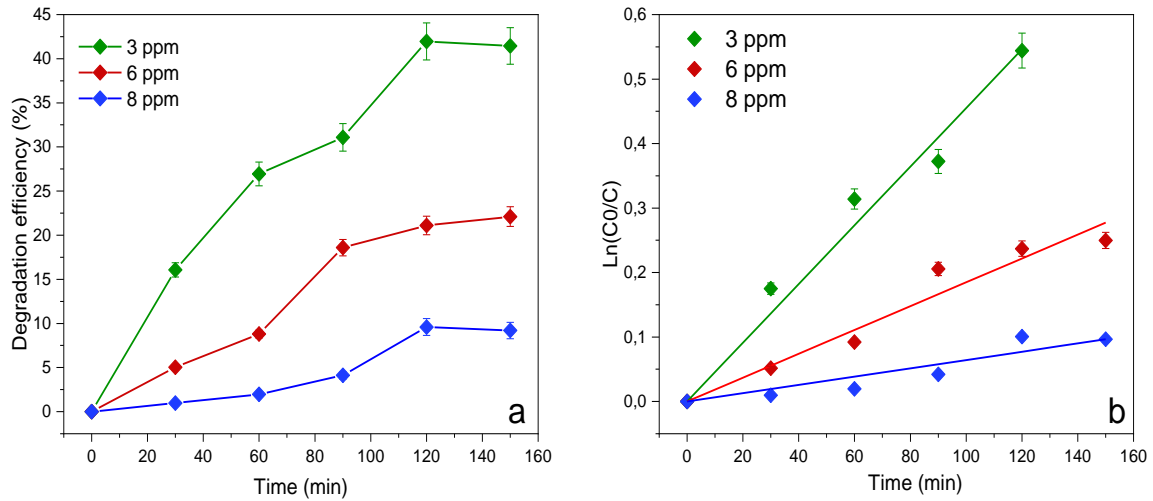


Figure 3. photocatalytic degradation kinetics modeling at different initial concentrations (C : Dye concentration in aqueous solution at any time t (mg/L), C_0 : Initial dye concentration in aqueous solution (mg/L) of methyl orange).

The pseudo-first-order model was examined for MO degradation kinetic. The value of reaction rate (k_1) was determined from the slope of a linear plot of $\ln(C_0/C)$ versus time, as shown in the Figure 3b. The R^2 values obtained from the fitting of PFO model are presented in Table 4. The reaction rate (k_1) increases with decreasing dye concentration. That finding aligns with a photocatalytic degradation of dyes [61]. The kinetic model of PFO is expressed as follows:

$$\ln\left(\frac{C_0}{C}\right) = K_{app} \cdot t \quad (5)$$

With C_0 and C as the concentrations expressed in mg/L, K_{app} is the reaction rate constant expressed in min. Table 4 suggests that the response charge decreases with growing dye concentration.

Table 4. Variation of the pseudo-first-order rate constant (K_1) at various initial concentration of methyl orange.

C_0 (mg/L)	K_{app} (min)	R^2
3	0.0046	0.99
6	0.0019	0.98
8	0.0006	0.94

3.3. Coupled adsorption and photocatalysis for complete elimination of dye

Different configurations were explored to assess the synergistic effect between adsorption and photocatalysis in MO removal from water. The adsorption of MO onto biochar was examined before photocatalysis, after photocatalysis (figures 4), and concurrently with photocatalysis (Figures 5). It was observed that the photocatalytic process enhanced MO removal following the adsorption step. This synergy between adsorption and photocatalysis, particularly under UV irradiation, resulted in a notable improvement in MO removal, consistent with prior research findings [62].

When photocatalysis was employed as a pretreatment (Fig. 4a), the removal efficiency increased from 25 to 40% as the treatment time was extended from 3 to 6 hours. Conversely, in the case of photocatalysis as a post-treatment (Fig. 4b), the removal rate increased only slightly, from 12 to 15%, with an extended treatment time of 6 hours. These results can be attributed to the high reaction rate observed at high MO concentrations during pretreatment (photocatalysis) and the slower reaction rate at low MO concentrations during post-treatment, where a notable portion of MO molecules had already been bound to the biochar during the initial adsorption step.

Furthermore, the synergistic effect of adsorption and photocatalysis played a crucial role in achieving excellent MO removal under UV irradiation. Biochar, acting as a photogenerated charge carrier, facilitated light absorption. By comparing Figure 4b with Figure 4d, it was evident that increasing the biochar dose enhanced removal efficiency, as more active sites for MO binding were provided [63]. Consequently, higher sorbent doses positively influenced the total removal efficiency of MO, with values of 96% and 100% achieved within 6 hours in Figure 4c and Figure 4d, respectively, due to the increased availability of active sites [64]. The intense interaction between biochar and methyl orange and the synergistic effects of adsorption and photocatalytic technologies contributed to this efficient removal process. Moreover, coupling reactions between these two techniques occurred in the presence of ample OH^\cdot radicals, leading to a low recombination rate of photogenerated electrons and holes [63].

Comparing the two processes, adsorption-photocatalysis, and photocatalysis-adsorption, it was observed that adsorption-photocatalysis was more efficient in removing and degrading MO. In other words, the synergistic effect notably enhanced MO's overall removal and/or degradation [38, 65].

Adsorption and photocatalysis are two complementary methods that can be applied either sequentially or simultaneously in the treatment of polluted waters. It has been reported that the concentration of methyl orange in wastewater typically ranges from 2 to 12 ppm [66], This is why a concentration of 6 ppm of methyl orange was selected for this study. Radiation is absorbed by TiO_2 and biochar particles, causing electrons to transition from the valence band (VB) of TiO_2 to the conduction band (CB), generating holes (h^+) and electrons along with other ROS [54, 67]. Photogenerated electrons are efficiently transferred from TiO_2 to biochar through a TiO_2 -biochar heterojunction, allowing for effective charge carrier separation. Following charge carrier separation, h^+ is captured by H_2O to form OH^\cdot , while photogenerated electrons react with O_2 to form $\text{O}_2^\cdot^-$ [68]. Biochar also acts as an electron acceptor, preventing the recombination of electron-hole pairs and enhancing photocatalytic efficiency [67].

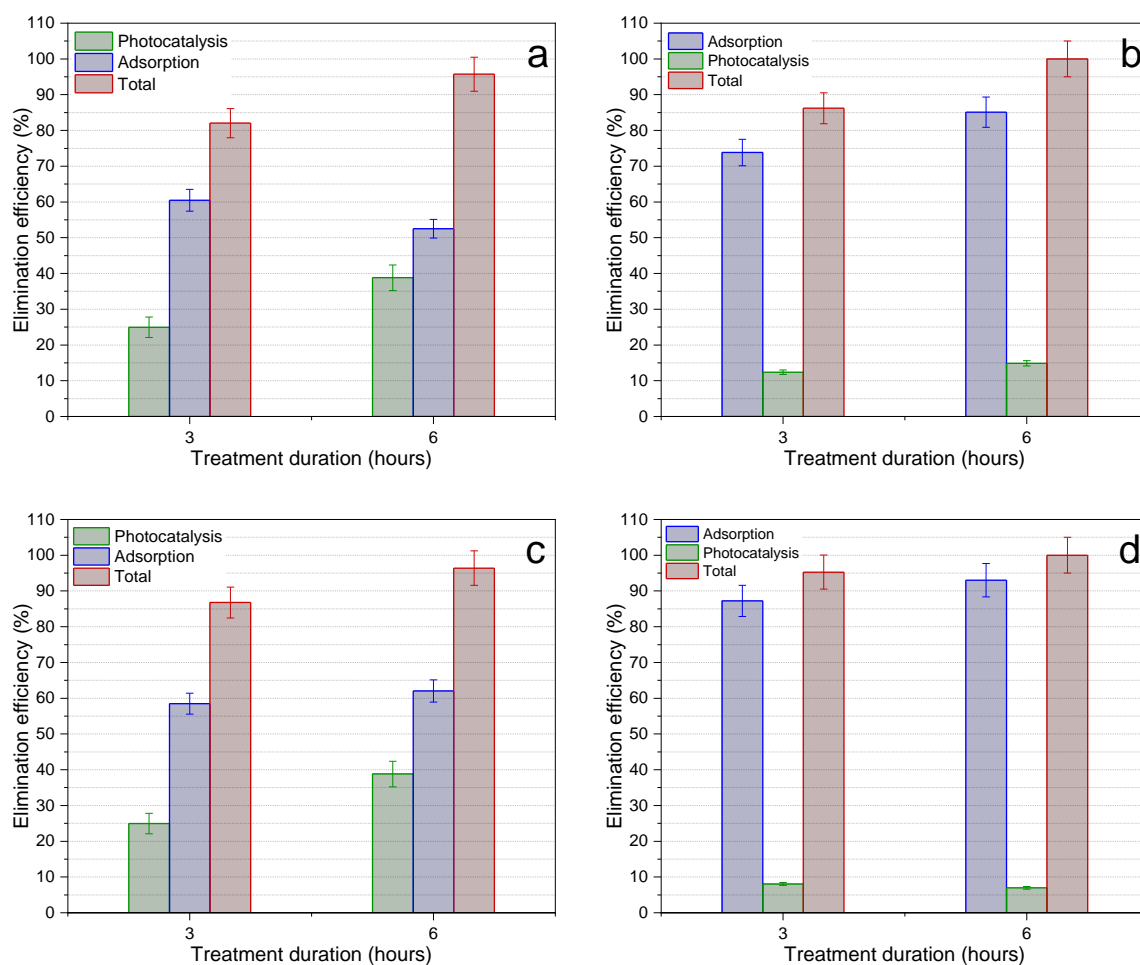


Figure 4. Combined photocatalysis-adsorption (a) for biochar dose of 80 mg/100mL, and adsorption-photocatalysis (b) for biochar dose of 80 mg/100mL, photocatalysis-

adsorption (c) for biochar dose of 100 mg/100mL, and adsorption-photocatalysis (d) for biochar dose of 100 mg/100mL.

Figure 5a shows a decrease in absorbance over time, reaching 0.021 a.u. after 6 hours, corresponding to a 95% MO elimination threshold, as shown in Figure 5b. This observation indicates that the dominating process is chemisorption, driven by the electrostatic interaction between the material's positive charge and the dye's negative charge [62]. When simultaneous adsorption and photodegradation were performed (as shown in Figure 5a), the removal rate of MO was even higher. This enhanced photodegradation rate, facilitated by synergistic oxidative adsorption photodegradation, shortens the migration paths of the reactive species [69]. Moreover, it broadens light absorption by blocking the photocatalytic active sites. The amount of biochar may obstruct light from reaching the TiO_2 surface and reduce MO decomposition [67].

These results suggest that biochar contributes to the adsorption process similarly to TiO_2 in the adsorption structure [62]. The simulation of synergistic adsorption and photocatalytic performance is achieved through enhanced mass transfer and photoelectron transfer of reactants in composites larger than TiO_2 , which densely grow on carbon spheres through in situ reactions [70].

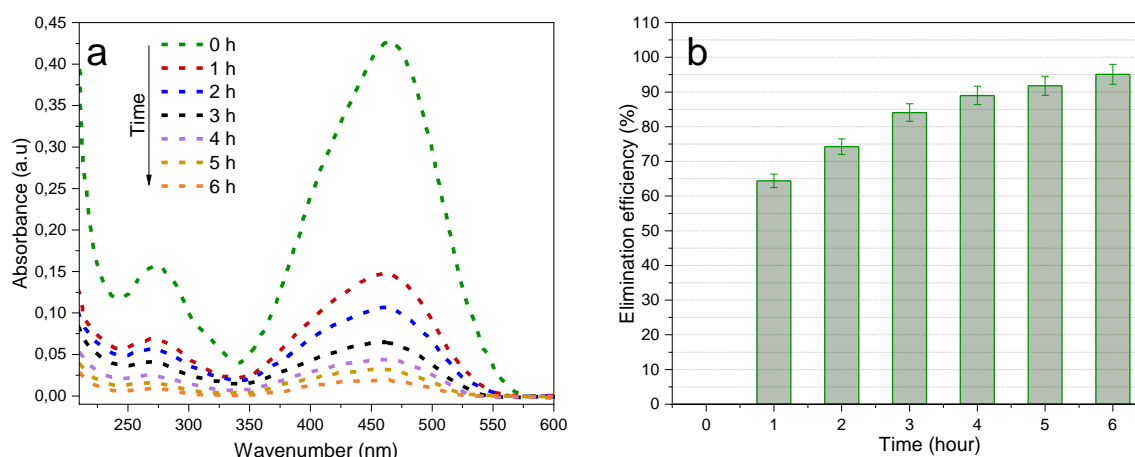


Figure 5. combined photocatalysis and adsorption at the same time (biochar dose: 100 mg/100mL, C_0 : 6 ppm, naturel pH).

Similar works were reported in the literature on removing different pollutants by combining adsorption and photocatalysis. Studies in the literature have explored the combined use of adsorption and photocatalysis for pollutant removal, employing

various materials as adsorbents and photocatalysts, as demonstrated in Table 5. From the reported total elimination efficiency (98-99%), the synergetic effect of these processes was efficient for eliminating different types of pollutants, even organic or inorganic ones. The obtained results are exciting; however, further optimization is needed.

Table 5. Similar work on the coupled adsorption-photocatalysis reported in literature.

Pollutant (concentration)	Adsorbent	Photocatalyst (treatment duration)	Total elimination efficiency (%)	Reference
Rhodamine B	Lignin biochar	BiOBr (180 min)	99.20	[64]
Antibiotics	Zr-SiO ₂	TiO ₂	98.11	[71]
CR	CoOx-CeO ₂	ZnO (65 min)	98.90	[65]
Hexavalent chromium	MXme	Zn-Al et TiO ₂ (90 min)	97.90	[38]
Rhodamine B	BiOx	TiO ₂ (40 min)	97.45	[72]
Methyl Orange (6 mg/L)	Biochar (80 mg/100mL)	TiO ₂ supported on cellulose (360 min)	Complete elimination	Present study
Methyl Orange (6 mg/L)	Biochar (100 mg/100mL)	TiO ₂ supported on cellulose (360 min)	Complete elimination	Present study

3.5. Effect of salts on the efficiency of adsorptive and photocatalytic processes

The effect of salts on adsorption and photocatalytic removal of MO has been realized to mimic the wastewater matrix. Various salts such as CuCl₂, ZnCl₂, SrCl₂, and MgCl₂ were mixed individually with MO solution, and the final concentration was fixed to 2 ppm. As evidenced, the process efficiency was determined for adsorption (3 hours) and photocatalysis (3 hours) and reported in Figure 6.

Figure 6 shows that the presence of these metal ions visibly affects both adsorption and photocatalytic efficiencies, as well as the action mechanism for activating the materials [73]. This figure shows that CuCl₂ is the most effective material for improving adsorption efficiency. Total removal capacity reaches 100% [74]. Then, CuCl₂, with its very high adsorption capacity [74], allowed a removal efficiency of 99.9% compared to SrCl₂ and ZnCl₂, achieving 93.9% and 98.5%, respectively. This

increase is due to the doping of chemical activators. These results allow us to conclude that the metal substantially increases the active site surface area. In addition to doping, TiO₂ can improve photocatalytic adsorption by forming complexes with support materials or chemical activators. Chemical activators, on the other hand, reduce the aggregation of biochar particles and/or TiO₂ nanoparticles over time and help overcome the problem of suspension recovery [75].

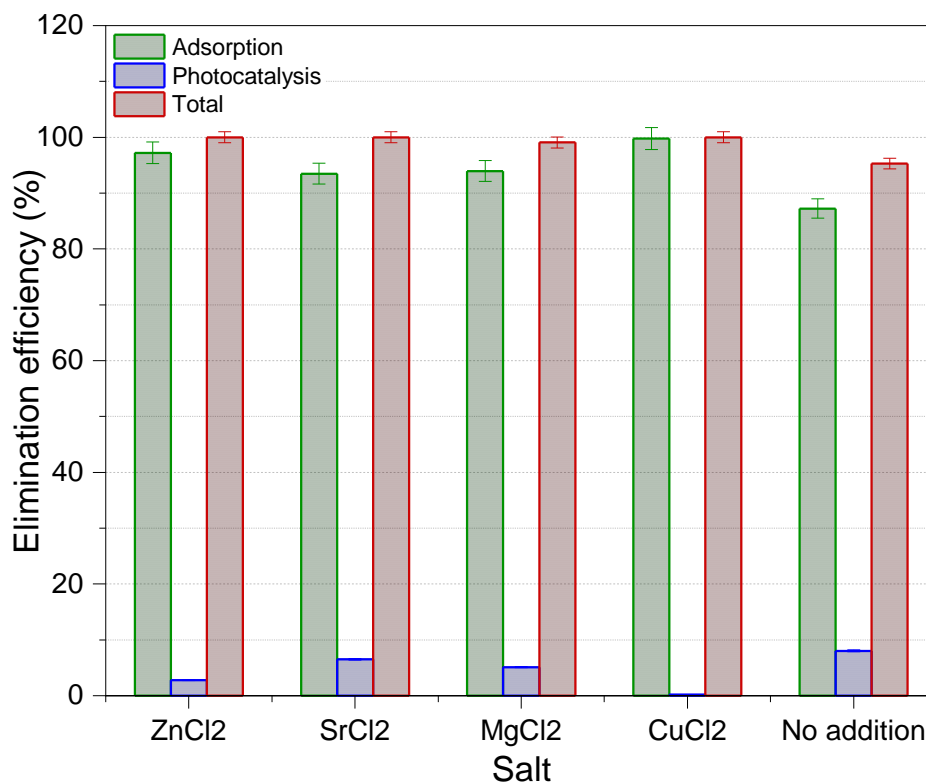


Figure 6. Effect of metal ions on the treatment efficiency of coupled adsorption-photocatalysis (biochar dose :100 mg/100mL, V_{solution} : 400 mL, [MO]: 6 ppm, treatment time: 3 hours, pH~7, [metal ion] = 2 ppm).

3.6. Effect of water types

Water is a natural source of human life each water sample has unique properties. The three types of water differ mainly by metal ion type and concentration content. This procedure tests the MO removal rate capability in three types of water: ultrapure water (UP) with a resistivity of 18.2, reverse osmosis water (DI) with a resistivity of 15.0, and tap water (TW).

Figure 7 shows that osmotic water is critical to remove the MO dye. The threshold is reached within 6 hours (3 hours adsorption, 3 hours photocatalysis) in DI water,

followed by tap water and ultrapure water. Tap water is usually treated with chlorine to make it safe for human consumption, but it can also contain harmful contaminants such as heavy metals and chemicals. Additionally, ultrapure water only contains H₂O and has a specific resistance of 18.2, making the reaction very slow [44]. Comparing adsorption and photocatalysis, Figure 7 shows that the efficiency of photocatalysis is relatively lower than that of adsorption. This finding indicates that adsorption is more effective and essential for different types of water and that biochar is protected from accidents. Evaluation of adsorption and photodegradation tests revealed that MO removal during adsorption was more effective than UV light after the same treatment time. The process features high removal efficiency, is environmentally friendly, has low energy costs, and is cost-effective due to separation and purification. [38].

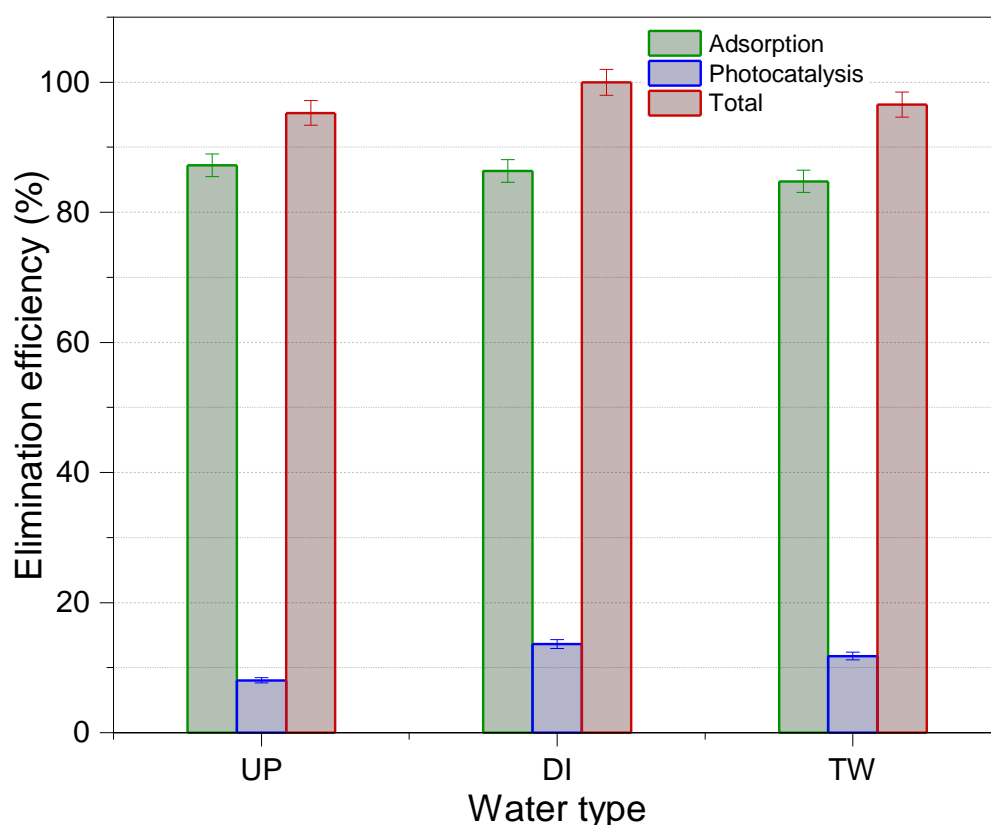


Figure 7. Effect of water types on the treatment efficiency of coupled adsorption-photocatalysis (biochar dose: 100 mg/100mL, V_{solution} : 400 mL, C_0 : 6 ppm, Treatment time: 3h adsorption, 3 h photocatalysis, naturel pH).

4. Conclusion

This article, introduced a chemical strategy to remove methyl orange (MO) from aqueous media by combining adsorption and photocatalytic processes. Research results reflect the effectiveness of this approach. The biochar used in the experiment showed remarkable performance in minimizing fouling. Bark biochar was successfully produced and characterized by techniques such as EDS and SEM, and subsequent applications proved highly efficient in reducing coloration.

The application of photocatalytic/adsorption configuration maximizes the simultaneous removal efficiency of MO, making it the most effective technique to remove MO from the ultrapure water matrix completely. The strong interaction observed between biochar and MO further demonstrates the synergy between these two technologies. This study investigated chemical strategies for removing MO from different types of water, including ultrapure water, osmotic, and tap water. Importantly, MO removal rates of 92.55, 100, and 96.55% were achieved for each water type. In particular, reverse osmosis water showed the highest MO removal rate, reaching 100% within 6 hours (3 hours of adsorption followed by 3 hours of photocatalysis) at a 100 mg/mL biochar dosage and an initial dye concentration of 6 ppm. Enhanced MO removal efficiency was observed with higher biochar dosage (from 80 mg/100 mL to 100 mg/100 mL) and longer treatment time (3 hours of adsorption followed by 3 hours of photocatalysis). Concerning the kinetic model, the results suggest that a pseudo-first-order model dominates the kinetics of MO adsorption in bark biochar. At the same time, photocatalysis was in better agreement with the pseudo-first-order model. Furthermore, the study identified the most efficient metal ions for MO removal in ultra-pure water, with the ranking as follows: 1) CuCl_2 , 2) ZnCl_2 , 3) SrCl_2 , and 4) MgCl_2 .

In summary, this study provides valuable insights into the effective removal of MO from various water at different degrees of purity (ultra-pure water (UP) with a resistivity of 18.2, reverse osmosis water (DI) with a resistivity of 15.0 and tap water (TW)) using a combination of adsorption and photocatalysis and provides the basis for potential applications in water treatment processes.

Declaration

Ethics approval and consent to participate

Not applicable

Consent for publication

Not applicable

Conflict of interest

The authors declare that they have no conflict of interest.

Funding

Not applicable

Availability of data and materials:

The datasets used and/or analyzed during the current study are available from the corresponding author on reasonable request.

References

- [1] H. Zeghioud, L. Fryda, H. Djelal, A. Assadi, A. Kane, A comprehensive review of biochar in removal of organic pollutants from wastewater: Characterization, toxicity, activation/functionalization and influencing treatment factors, *J. Water Process Eng.* 47 (2022). <https://doi.org/10.1016/j.jwpe.2022.102801>.
- [2] R.O. Alves de Lima, A.P. Bazo, D.M.F. Salvadori, C.M. Rech, D. de Palma Oliveira, G. de Aragão Umbuzeiro, Mutagenic and carcinogenic potential of a textile azo dye processing plant effluent that impacts a drinking water source, *Mutat. Res. - Genet. Toxicol. Environ. Mutagen.* 626 (2007) 53–60.
<https://doi.org/10.1016/j.mrgentox.2006.08.002>.
- [3] H. Zeghioud, P. Nguyen-Tri, L. Khezami, A. Amrane, A.A. Assadi, Review on discharge Plasma for water treatment: mechanism, reactor geometries, active species and combined processes, *J. Water Process Eng.* 38 (2020) 101664.
<https://doi.org/10.1016/j.jwpe.2020.101664>.
- [4] P. Li, Q. Cai, W. Lin, B. Chen, B. Zhang, Offshore oil spill response practices and emerging challenges, *Mar. Pollut. Bull.* 110 (2016) 6–27.
<https://doi.org/10.1016/j.marpolbul.2016.06.020>.
- [5] J.H. Park, Y.S. Ok, S.H. Kim, J.S. Cho, J.S. Heo, R.D. Delaune, D.C. Seo, Competitive adsorption of heavy metals onto sesame straw biochar in aqueous solutions, *Chemosphere.* 142 (2016) 77–83.
<https://doi.org/10.1016/j.chemosphere.2015.05.093>.

- [6] A. Javed, A. Mushtaq, A critical review of electrocoagulation and other electrochemical methods, 23 (2023) 98–110.
- [7] Darban, A.K.; Shahedi, A.; Taghipour, F.; Jamshidi-Zanjani, A. (2020). A review on industrial wastewater treatment via electrocoagulation processes. *Current Opinion in Electrochemistry*, (), S2451910320301095. doi: 10.1016/j.coelec.2020.05.009.
- [8] U. Advanced, O. Processes, A Review on the Treatment of Petroleum Refinery Wastewater Using Advanced Oxidation Processes, (2021) 1–29.
- [9] D. Luo, L. Wang, H. Nan, Y. Cao, H. Wang, T.V. Kumar, C. Wang, Phosphorus adsorption by functionalized biochar: a review, *Environmental Chemistry Letters* volume 21, pages497–524 (2023).
- [10] G. Gan, S. Fan, X. Li, Z. Zhang, Z. Hao, Adsorption and membrane separation for removal and recovery of volatile organic compounds, *Journal of Environmental Sciences*, Volume 123, January 2023, Pages 96-115.
- [11] J. Soli, S. Kachbouri, E. Elaloui, C. Charnay Role of surfactant type on morphological, textural, optical, and photocatalytic properties of ZnO nanoparticles obtained by modified sol–gel. *Journal of Sol-Gel Science and Technology* 100 (2021) 271–285 <https://doi.org/10.1007/s10971-021-05653-4> .
- [12] T. Munawar, S. Sardar, F. Mukhtar, M. S. Nadeem, S. Manzoor, M. N. Ashiq, S. A. Khan, M. Koc, F. Iqbal, Fabrication of fullerene-supported La₂O₃–C₆₀ nanocomposites: dual-functional materials for photocatalysis and supercapacitor electrodes, *Physical Chemistry Chemical Physics*, issue 9, 2023.
- [13] X. Jia, Z. Li, C. Wang, K. Li, L. Zhang, D. Ji'an, Study of the dynamics of material removal processes in combined pulse laser drilling of alumina ceramic, *Optics & Laser Technology*. Volume 160, May 2023, 109053.
- [14] S. Kim, S.N. Nam, A. Jang, M. Jang, C.M. Park, A. Son, N. Her, J. Heo, Y. Yoon, Review of adsorption–membrane hybrid systems for water and wastewater treatment, *Chemosphere*. 286 (2022) 131916. <https://doi.org/10.1016/j.chemosphere.2021.131916>.
- [15] B. Lellis, C. Z. Fávaro-Polonio, J. A. Pamphile and J. C. Polonio, Effects of textile dyes on health and the environment, *Biotechnol. Res. Innov.* 3 (2019) 275 — 290
- [16] S. Dutta, B. Gupta, S. K. Srivastava, A. K. Gupta, Recent advances on the removal of dyes from wastewater using various adsorbents: a critical review, *Mater.*

Adv. 2 (2021), 4497.

[17] H. Zeghioud, S. Mouhamadou, Dye Removal Characteristics of Magnetic Biochar Derived from Sewage Sludge: Isotherm, Thermodynamics, Kinetics, and Mechanism, *Water, Air, Soil Pollut.* (2023). <https://doi.org/10.1007/s11270-023-06251-6>.

[18] P.R. Yaashikaa, P.S. Kumar, S. Varjani, A. Saravanan, A critical review on the biochar production techniques, characterization, stability and applications for circular bioeconomy, *Biotechnol. Reports.* 28 (2020) e00570.

<https://doi.org/10.1016/j.btre.2020.e00570>.

[19] X. Li, J. Zhang, B. Liu, Z. Su, A critical review on the application and recent developments of post-modified biochar in supercapacitors, *J. Clean. Prod.* 310 (2021) 127428. <https://doi.org/10.1016/j.jclepro.2021.127428>.

[20] K. Luo, Y. Pang, D. Wang, X. Li, L. Wang, M. Lei, Q. Huang, Q. Yang, A critical review on the application of biochar in environmental pollution remediation: Role of persistent free radicals (PFRs), *J. Environ. Sci. (China).* 108 (2021) 201–216.

<https://doi.org/10.1016/j.jes.2021.02.021>.

[21] A. Othmani, J. John, H. Rajendran, A. Mansouri, M. Sillanpää, P. VelayudhaperumalChellam, Biochar and activated carbon derivatives of lignocellulosic fibers towards adsorptive removal of pollutants from aqueous systems: Critical study and future insight, *Sep. Purif. Technol.* 274 (2021) 119062.

<https://doi.org/10.1016/j.seppur.2021.119062>.

[22] Y. Li, H. Yu, L. Liu, H. Yu, Application of co-pyrolysis biochar for the adsorption and immobilization of heavy metals in contaminated environmental substrates, *J. Hazard. Mater.* 420 (2021) 126655.

<https://doi.org/10.1016/j.jhazmat.2021.126655>.

[23] M. Guo, W. Song, J. Tian, Biochar-Facilitated Soil Remediation: Mechanisms and Efficacy Variations, *Front. Environ. Sci.* 8 (2020).

<https://doi.org/10.3389/fenvs.2020.521512>.

[24] Johannes Lehmann and Stephen Joseph, *Biochar for Environmental Management*, 2009.

[25] Z. Abbas, S. Ali, M. Rizwan, I.E. Zaheer, A. Malik, M.A. Riaz, M.R. Shahid, M.Z. ur Rehman, M.I. Al-Wabel, A critical review of mechanisms involved in the adsorption of organic and inorganic contaminants through biochar, *Arab. J. Geosci.* 11 (2018).

<https://doi.org/10.1007/s12517-018-3790-1>.

- [26] Y. Zhou, S. Qin, S. Verma, T. Sar, S. Sarsaiya, B. Ravindran, T. Liu, R. Sindhu, A.K. Patel, P. Binod, S. Varjani, R. Rani Singhnia, Z. Zhang, M.K. Awasthi, Production and beneficial impact of biochar for environmental application: A comprehensive review, *Bioresour. Technol.* 337 (2021) 125451. <https://doi.org/10.1016/j.biortech.2021.125451>.
- [27] M. Patel, R. Kumar, C.U. Pittman, D. Mohan, Ciprofloxacin and acetaminophen sorption onto banana peel biochars: Environmental and process parameter influences, *Environ. Res.* 201 (2021) 111218. <https://doi.org/10.1016/j.envres.2021.111218>.
- [28] S.S. Mayakaduwa, P. Kumarathilaka, I. Herath, M. Ahmad, M. Al-Wabel, Y.S. Ok, A. Usman, A. Abduljabbar, M. Vithanage, Equilibrium and kinetic mechanisms of woody biochar on aqueous glyphosate removal, *Chemosphere.* 144 (2016) 2516–2521. <https://doi.org/10.1016/j.chemosphere.2015.07.080>.
- [29] A. Aidan, Parametric Study of Methyl Orange Removal Using Metal – Organic Frameworks Based on Factorial Experimental Design Analysis, *Energies.* 15 (2022) 4642.
- [30] R. Jemai, M.A. Djebbi, S. Boubakri, H. Ben Rhaiem, A. Ben, H. Amara, Effective Removal of Methyl Orange Dyes Using an Adsorbent Prepared from Porous Starch Aerogel and Organoclay, *Colorants.* 2 (2023) 209–229.
- [31] G.C. De Assis, E. Skovroinski, V.D. Leite, M.O. Rodrigues, A. Galembeck, M.C.F. Alves, J. Eastoe, R.J. De Oliveira, Conversion of “waste Plastic” into Photocatalytic Nanofoams for Environmental Remediation, *ACS Appl. Mater. Interfaces.* 10 (2018) 8077–8085. <https://doi.org/10.1021/acsami.7b19834>.
- [32] H. Yi, D. Huang, L. Qin, G. Zeng, C. Lai, M. Cheng, S. Ye, B. Song, X. Ren, X. Guo, Selective prepared carbon nanomaterials for advanced photocatalytic application in environmental pollutant treatment and hydrogen production, *Appl. Catal. B Environ.* 239 (2018) 408–424. <https://doi.org/10.1016/j.apcatb.2018.07.068>.
- [33] C. Zhou, C. Lai, C. Zhang, G. Zeng, D. Huang, M. Cheng, L. Hu, W. Xiong, M. Chen, J. Wang, Y. Yang, L. Jiang, Semiconductor/boron nitride composites: Synthesis, properties, and photocatalysis applications, *Appl. Catal. B Environ.* 238 (2018) 6–18. <https://doi.org/10.1016/j.apcatb.2018.07.011>.
- [34] P. Mehdizadeh, M. Jamdar, M. A. Mahdi, W. K. Abdulsahib, L. S. Jasim, S. R. Yousefi, M. Si. Niasari, nanocomposites based on Tb-Co-O nanostructures and their application as photocatalysts under UV/Visible light for removal of organic pollutants

in water, *Arabian Journal of Chemistry* 16, 4, 2023, 104579.

[35] Q. Liang, X. Liu, G. Zeng, Z. Liu, L. Tang, B. Shao, Z. Zeng, W. Zhang, Y. Liu, M. Cheng, W. Tang, S. Gong, Surfactant-assisted synthesis of photocatalysts: Mechanism, synthesis, recent advances and environmental application, *Chem. Eng. J.* 372 (2019) 429–451. <https://doi.org/10.1016/j.cej.2019.04.168>.

[36] J. Li, L. Xu, J. He, P. Zhou, L. Hu, D. Li, B. Wang, The Structure feature of novel Cu₂O/ e -HTi₂NbO₇ nanocomposite and their enhanced photocatalytic activity, *Nano.* 12 (2017) 1–10. <https://doi.org/10.1142/S1793292017501004>.

[37] W. Zhen, X. Ning, B. Yang, Y. Wu, Z. Li, G. Lu, The enhancement of CdS photocatalytic activity for water splitting via anti-photocorrosion by coating Ni₂P shell and removing nascent formed oxygen with artificial gill, *Appl. Catal. B Environ.* 221 (2018) 243–257. <https://doi.org/10.1016/j.apcatb.2017.09.024>.

[38] N.S. Jamaluddin, N.H. Alias, S. Samitsu, N.H. Othman, J. Jaafar, F. Marpani, W.J. Lau, Y.Z. Tan, Efficient chromium (VI) removal from wastewater by adsorption-assisted photocatalysis using MXene, *J. Environ. Chem. Eng.* 10 (2022) 108665. <https://doi.org/10.1016/j.jece.2022.108665>.

[39] C. Li, B. Zhang, X. Jin, Y. Wang, Y. Zheng, Excellent integrated adsorption and photocatalysis of a black BiOBr for fast removal dyes: A case of carbon species and oxygen vacancies synergistic effect, *Appl. Surf. Sci.* 577 (2022) 151920. <https://doi.org/10.1016/j.apsusc.2021.151920>.

[40] C. Liu, C. Zhu, H. Wang, S. Xie, J. Zhou, H. Fang, Synergistic removal of organic pollutants by Co-doped MIL-53(Al) composite through the integrated adsorption/photocatalysis, *J. Solid State Chem.* 316 (2022) 123582. <https://doi.org/10.1016/j.jssc.2022.123582>.

[41] K. Kaetzl, M. Lübken, E. Nettmann, S. Krimmler, M. Wichern, Slow sand filtration of raw wastewater using biochar as an alternative filtration media, *Sci. Rep.* 10 (2020) 1–11. <https://doi.org/10.1038/s41598-020-57981-0>.

[42] H. Zeghioud, A.A. Assadi, N. Khellaf, H. Djelal, A. Amrane, S. Rtimi, Reactive species monitoring and their contribution for removal of textile effluent with photocatalysis under UV and visible lights: Dynamics and mechanism, *J. Photochem. Photobiol. A Chem.* 365 (2018) 94–102. <https://doi.org/10.1016/j.jphotochem.2018.07.031>.

[43] A.G. Adeniyi, J.O. Ighalo, D.V. Onifade, Biochar from the Thermochemical Conversion of Orange (*Citrus sinensis*) Peel and Albedo: Product Quality and

Potential Applications, *Chem. Africa*. 3 (2020) 439–448.

<https://doi.org/10.1007/s42250-020-00119-6>.

[44] P. Guillaume, Caractérisation biochimique d'exopolymères d'origine algale du bassin de Marennes-Oléron et étude des propriétés physico-chimiques de surface de micro-organismes impliquées dans leur adhésion, Thèse. (2010) 323 p.

[45] S. Gupta, P. Krishnan, A. Kashani, H.W. Kua, Application of biochar from coconut and wood waste to reduce shrinkage and improve physical properties of silica fume-cement mortar, *Constr. Build. Mater.* 262 (2020) 120688.

<https://doi.org/10.1016/j.conbuildmat.2020.120688>.

[46] A.S. Yusuff, M.A. Lala, K.A. Thompson-Yusuff, E.O. Babatunde, ZnCl₂-modified eucalyptus bark biochar as adsorbent: preparation, characterization and its application in adsorption of Cr(VI) from aqueous solutions, *South African J. Chem. Eng.* 42 (2022) 138–145. <https://doi.org/10.1016/j.sajce.2022.08.002>.

[47] T. Yang, Y. Xu, Q. Huang, Y. Sun, X. Liang, L. Wang, X. Qin, L. Zhao, Adsorption characteristics and the removal mechanism of two novel Fe-Zn composite modified biochar for Cd(II) in water, *Bioresour. Technol.* 333 (2021) 125078.

<https://doi.org/10.1016/j.biortech.2021.125078>.

[48] S. Melouki, A. Reffasi, A. Merrouche, L. Reinert, L. Duclaux, Common reed biochars for the adsorption of methyl orange in aqueous solution | Biochars issus de roseau commun pour l'adsorption du méthylorange en solution aqueuse, *Rev. Des Sci. l'Eau*. 32 (2020) 349–367.

[49] E. Black, T.E. Design, F. Hassan, P. Bonnet, J. Marie, D. Dikdim, N.G. Bandjoun, C. Caperaa, S. Dalhatou, A. Kane, H. Zeghioud, Photocatalytic Degradation of Bromophenol Blue and Reactive Oxygen Species Contribution, (2022).

[50] X. Yao, L. Ji, J. Guo, S. Ge, W. Lu, Y. Chen, L. Cai, Y. Wang, W. Song, An abundant porous biochar material derived from wakame (*Undariapinnatifida*) with high adsorption performance for three organic dyes, *Bioresour. Technol.* 318 (2020) 124082. <https://doi.org/10.1016/j.biortech.2020.124082>.

[51] X. Li, J. Xu, X. Luo, J. Shi, Efficient adsorption of dyes from aqueous solution using a novel functionalized magnetic biochar: Synthesis, kinetics, isotherms, adsorption mechanism, and reusability, *Bioresour. Technol.* 360 (2022) 127526.

<https://doi.org/10.1016/j.biortech.2022.127526>.

[52] A.Rashidinia , M. Dinari, An amine-rich porous organic polymer with flexible

diarylmethane moieties for adsorptive removal of anionic dyes, *New Journal of Chemistry*, 2023. <https://doi.org/10.1039/D3NJ02678G>.

[53] O. Pezoti, A.L. Cazetta, K.C. Bedin, L.S. Souza, A.C. Martins, T.L. Silva, O.O. Santos Júnior, J. V. Visentainer, V.C. Almeida, NaOH-activated carbon of high surface area produced from guava seeds as a high-efficiency adsorbent for amoxicillin removal: Kinetic, isotherm and thermodynamic studies, *Chem. Eng. J.* 288 (2016) 778–788. <https://doi.org/10.1016/j.cej.2015.12.042>.

[54] Y.H. Chiu, T.F.M. Chang, C.Y. Chen, M. Sone, Y.J. Hsu, Mechanistic insights into photodegradation of organic dyes using heterostructure photocatalysts, *Catalysts*. 9 (2019). <https://doi.org/10.3390/catal9050430>.

[55] P.G.T.N. Dhas, H. Gulyas, R. Otterpohl, Impact of Powdered Activated Carbon and Anion Exchange Resin on Photocatalytic Treatment of Textile Wastewater, *J. Environ. Prot. (Irvine, Calif.)*. 06 (2015) 191–203.

<https://doi.org/10.4236/jep.2015.63020>.

[57] Z.S. Khalifa, M. Shaban, Blue Dyes by Engineering the Surface Nano-Textures of TiO₂, (2023).

[58] C.H. Nguyen, C.C. Fu, R.S. Juang, Degradation of methylene blue and methyl orange by palladium-doped TiO₂ photocatalysis for water reuse: Efficiency and degradation pathways, *J. Clean. Prod.* 202 (2018) 413–427.

<https://doi.org/10.1016/j.jclepro.2018.08.110>.

[59] N.O. Eddy, R.A. Ukpe, P. Ameh, R. Ogbodo, R. Garg, R. Garg, Theoretical and experimental studies on photocatalytic removal of methylene blue (MetB) from aqueous solution using oyster shell synthesized CaO nanoparticles (CaONP-O), *Environ. Sci. Pollut. Res.* 30 (2022) 81417–81432. <https://doi.org/10.1007/s11356-022-22747-w>.

[60] S. Alkaykh, A. Mbarek, E.E. Ali-Shattle, Photocatalytic degradation of methylene blue dye in aqueous solution by MnTiO₃ nanoparticles under sunlight irradiation, *Heliyon*. 6 (2020) e03663. <https://doi.org/10.1016/j.heliyon.2020.e03663>.

[61] Y. Xu, C.H. Langford, Variation of Langmuir adsorption constant determined for TiO₂-photocatalyzed degradation of acetophenone under different light intensity, *J. Photochem. Photobiol. A Chem.* 133 (2000) 67–71. [https://doi.org/10.1016/S1010-6030\(00\)00220-3](https://doi.org/10.1016/S1010-6030(00)00220-3).

[62] A. Hetero-structures, L. Andronic, L. Isac, C. Cazan, applied sciences Simultaneous Adsorption and Photocatalysis Processes Based on Ternary TiO₂ –

Cu x S – Fly, (2020).

- [63] Y. Qing, Y. Li, Z. Guo, Y. Yang, W. Li, Photocatalytic Bi₂WO₆/pg-C₃N₄-embedded in polyamide microfiltration membrane with enhanced performance in synergistic adsorption-photocatalysis of 17β-estradiol from water, *J. Environ. Chem. Eng.* 10 (2022) 108648. <https://doi.org/10.1016/j.jece.2022.108648>.
- [64] Q. Yang, X. Li, Q. Tian, A. Pan, X. Liu, H. Yin, Y. Shi, G. Fang, Synergistic effect of adsorption and photocatalysis of BiOBr/lignin-biochar composites with oxygen vacancies under visible light irradiation, *J. Ind. Eng. Chem.* 117 (2022) 117–129. <https://doi.org/10.1016/j.jiec.2022.09.044>.
- [65] S. Lu, Y. Ma, L. Zhao, Production of ZnO-CoOx-CeO₂ nanocomposites and their dye removal performance from wastewater by adsorption-photocatalysis, *J. Mol. Liq.* 364 (2022) 119924. <https://doi.org/10.1016/j.molliq.2022.119924>.
- [66] S. Rajendrachari, N. Basavegowda, Vinaykumar, D. Narsimhachary, P. Somu, M.-J. Lee, Electrochemical determination of methyl orange dye using mechanically alloyed novel metallic glass modified carbon paste electrode by cyclic voltammetry *Inorganic Chemistry Communications*, 155, 2023, 111010. (<https://doi.org/10.1016/j.inoche.2023.111010>).
- [67] Y. Jiang, A. Liu, Cornstalk biochar-TiO₂ composites as alternative photocatalyst for degrading methyl orange, *Environ. Sci. Pollut. Res.* 30 (2023) 31923–31934. <https://doi.org/10.1007/s11356-022-24490-8>.
- [68] L. V. Trandafilović, D.J. Jovanović, X. Zhang, S. Ptasińska, M.D. Dramićanin, Enhanced photocatalytic degradation of methylene blue and methyl orange by ZnO:Eu nanoparticles, *Appl. Catal. B Environ.* 203 (2017) 740–752. <https://doi.org/10.1016/j.apcatb.2016.10.063>.
- [69] R. Venkatesh, P.R. Sekaran, K. Udayakumar, D. Jagadeesh, K. Raju, M.B. Bayu, Adsorption and Photocatalytic Degradation Properties of Bimetallic Ag/MgO/Biochar Nanocomposites, *Adsorpt. Sci. Technol.* 2022 (2022). <https://doi.org/10.1155/2022/3631584>.
- [70] X. Feng, L. Gu, N. Wang, Q. Pu, G. Liu, Fe/N co-doped nano-TiO₂ wrapped mesoporous carbon spheres for synergistically enhanced adsorption and photocatalysis, *J. Mater. Sci. Technol.* 135 (2023) 54–64. <https://doi.org/10.1016/j.jmst.2022.06.038>.
- [71] Y. Yu, X. Hu, M. Li, J. Fang, C. Leng, X. Zhu, W. Xu, J. Qin, L. Yao, Z. Liu, Z. Fang, Constructing mesoporous Zr-doped SiO₂ onto efficient Z-scheme TiO₂/g-C₃N₄

heterojunction for antibiotic degradation via adsorption-photocatalysis and mechanism insight, *Environ. Res.* 214 (2022) 114189.

<https://doi.org/10.1016/j.envres.2022.114189>.

[72] S. Yao, J. Wang, X. Zhou, S. Zhou, X. Pu, W. Li, One-pot low-temperature synthesis of BiO_x/TiO₂ hierarchical composites of adsorption coupled with photocatalysis for quick degradation of colored and colorless organic pollutants, *Adv. Powder Technol.* 31 (2020) 1924–1932. <https://doi.org/10.1016/j.apt.2020.02.023>.

[73] Z. Yuan, Z. Xu, D. Zhang, W. Chen, T. Zhang, Y. Huang, L. Gu, H. Deng, D. Tian, Box-Behnken design approach towards optimization of activated carbon synthesized by co-pyrolysis of waste polyester textiles and MgCl₂, *Appl. Surf. Sci.* 427 (2018) 340–348. <https://doi.org/10.1016/j.apsusc.2017.08.241>.

[74] G.S. dos Reis, M. Guy, M. Mathieu, M. Jebrane, E.C. Lima, M. Thyrel, G.L. Dotto, S.H. Larsson, A comparative study of chemical treatment by MgCl₂, ZnSO₄, ZnCl₂, and KOH on physicochemical properties and acetaminophen adsorption performance of biobased porous materials from tree bark residues, *Colloids Surfaces A Physicochem. Eng. Asp.* 642 (2022) 128626. <https://doi.org/10.1016/j.colsurfa.2022.128626>.

[75] H. Bel Hadjtaief, A. Omri, M. Ben Zina, P. Da Costa, M.E. Galvez, Titanium Dioxide Supported on Different Porous Materials as Photocatalyst for the Degradation of Methyl Green in Wastewaters, *Adv. Mater. Sci. Eng.* 2015 (2015). <https://doi.org/10.1155/2015/759853>.